Hindawi
Wireless Communications and Mobile Computing
Volume 2020, Article ID 3812826, 12 pages
https://doi.org/10.1155/2020/3812826

Research Article

Performance Analysis of IQI Impaired Cooperative NOMA for 5G-Enabled Internet of Things

Hui Guo,[1] Xuejiao Guo,[1] Chao Deng,[1] and Shangqing Zhao[2]

[1]*School of Physics and Electronic Information Engineering, Henan Polytechnic University, Jiaozuo 454000, China*
[2]*Department of Electrical Engineering, University of South Florida, Tampa, FL 33620, USA*

Correspondence should be addressed to Chao Deng; super@hpu.edu.cn

Received 3 January 2020; Revised 22 February 2020; Accepted 11 June 2020; Published 13 July 2020

Academic Editor: Hien Quoc Ngo

This paper investigates the joint effects of in-phase and quadrature-phase imbalance (IQI) and imperfect successive interference cancellation (ipSIC) on the cooperative Internet of Things (IoT) nonorthogonal multiple access (NOMA) networks where the Nakagami-*m* fading channel is taken into account. The closed-form expressions of outage probability for the far and near IoT devices are derived to evaluate the outage behaviors. For deeper insights of the performance of the considered system, the approximate outage probability and diversity order in high signal-to-noise ratio (SNR) regime are obtained. In addition, we also analyze the throughput and energy efficiency to characterize the performance of the considered system. The simulation results demonstrate that, compared with IQI, ipSIC has a greater impact on the outage performance for the near-IoT-device of the considered system. Furthermore, we also find that the outage probabilities of IoT devices can be minimized by selecting a specific power allocation scheme.

1. Introduction

With the development of Internet of Things (IoT), traditional orthogonal multiple access (OMA) can no longer afford massive connections due to its low spectrum utilization [1]. The proposals of massive multiple-input multiple-output (MIMO) [2], small cell networks (SCNs) [3], millimeter wave (mmWave) [4], nonorthogonal multiple access (NOMA) [5], and some other 5G-related technologies have made it possible to implement the IoT [6]. Among these technologies, NOMA has been accepted by the Third Generation Partnership Project (3GPP) due to the fact that it can serve multiple devices simultaneously without neglecting fairness [7]. Traditional OMA is required to use orthogonal resources to support multiple devices, while relying on the power multiplexing of NOMA IoT can serve a large number of various devices in the same time/frequency domain [8, 9]. Furthermore, the physical layer security performance of NOMA systems outperforms the OMA system and improves the security rate of the system greatly [10]. In addition, to ensure the fairness among devices, different power signals are transmitted according to the channel state information (CSI) between the transmitter (TX) and receiver (RX), and the successive interference cancellation (SIC) is adopted at the RX to eliminate interdevice interference [11, 12].

To further enhance the robustness and expand coverage, cooperative relay communication has been introduced into NOMA systems [13–17]. In [13], cooperative relay was taken into account in the NOMA systems, and it has been proved that the proposed scheme can reduce the outage probability and increase the diversity gain of the systems. In order to improve the spectral efficiency, the authors of [14] proposed a new cooperative NOMA transmission scheme in the cognitive radio systems and derived the exact closed-form expressions for outage probability. The outage performance of cooperative NOMA amplify-and-forward (AF) and decode-and-forward (DF) system with a single user was studied in [15], and the results showed that the relay in AF protocol outperforms the relay in DF protocol. In [16], the outage probability of cooperative NOMA system over Rayleigh channels was analyzed where the near user acted as a DF relay. Particularly, the cooperative NOMA network in the

IoT was proposed in [17]; the average throughput and the diversity order were analyzed to characterize the system. In [18], the authors proposed a cooperative NOMA scheme in which the near user acts as a DF relay and the analytical expression of intercept probability was derived to evaluate the system. All of the above studies showed that the cooperative NOMA can improve the system performance. As the core technology of NOMA, SIC has well performance on signal detection, while at the expense of the complexity of RX [19]. To this end, a host of works has drawn attention to imperfect SIC (ipSIC) ([20–23] and references therein). Authors in [20] proposed a more practical network in which ipSIC was considered in the cooperative NOMA system, and the closed-form expressions of the outage probability were derived. In [21], the authors presented the closed-form expressions of outage probability and ergodic sum rate of the cooperative AF NOMA over Nakagami-m channels by considering ipSIC in the network. In addition, the effects of ipSIC on the two-way and cognitive radio NOMA system were studied in [22, 23], respectively. All of these articles are instructive for the practical NOMA systems.

The aforementioned works mainly focused on the perfect radio frequency (RF) which is overidealistic. In practice, in-phase and quadrature-phase imbalance (IQI) inevitably occurs due to component mismatch or manufacturing process problems [24]. Although the influence of IQI can be mitigated by compensation algorithms and correction algorithms, it cannot be completely eliminated due to the different forms of noise [25–28]. The authors in [29] have demonstrated that IQI has negative effects on the NOMA systems and cannot be ignored. To solve this problem, authors in [30] studied the impact of IQI on the two-way cooperative AF relay systems and derived the closed-form and asymptotic expressions for the outage probability. The effects of TX IQI, RX IQI, and joint TX/RX IQI on the outage performance of the single-hop NOMA system were compared in [31]. The performance of cooperative NOMA system with IQI at the relay was analyzed by deriving closed-form expressions for the outage probability [32]. Recently, the impact of IQI on the cooperative NOMA DF network over Rayleigh channels has been considered in [33], while the influence of IQI on the source node was not taken into account. Moreover, the direct link between the source and the far user was not considered in [33].

Motivated by the previous discussion, in this paper, we discuss the effect of IQI on the cooperative IoT NOMA AF relaying system over Nakagami-m fading channels, and ipSIC is taken into account as well. In the considered system, the source node can communicate with the destination nodes with the aid of an AF relay or directly. To demonstrate the performance of the considered system, the exact analytical expressions of the outage probability are derived. In order to gain more insights, asymptotic analyses and diversity orders are calculated. Finally, the throughput and energy efficiency are also performed. The main contributions of this paper are summarized as follows:

(i) The exact outage probability expressions of the near-IoT-device and far-IoT-device of the considered system are derived by considering IQI at source, relay, and IoT devices; meanwhile, ipSIC is taken into account

(ii) In order to obtain more insights, the asymptotic outage performance is analyzed. For more intuitive evaluation of the considered system performance, the diversity order is further obtained

(iii) Finally, we deduce the throughput and energy efficiency of the considered network. The results confirm that (1) the system throughput will increase when the signal-to-noise ratio (SNR) is increasing, while approaches to a fixed value in the high SNR regime; (2) the energy efficiency will increase all the time in the ideal conditions, while in the non-ideal conditions, the energy efficiency will reach the upper bound due to the existence of IQI and ipSIC

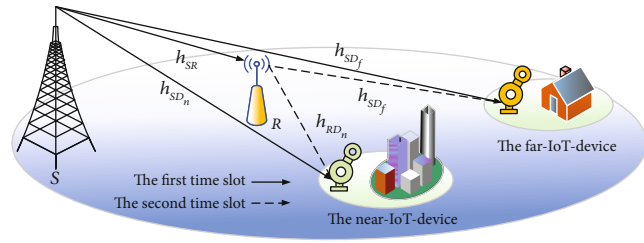

Figure 1: System model of cooperative IoT NOMA networks.

The rest of this paper is organized as follows. Section 2 describes the cooperative IoT NOMA systems with IQI and ipSIC; Section 3 discusses the exact and asymptotic outage performance, the diversity order, the system throughput, and the energy efficiency. The numerical results are presented in Section 4 before we conclude the paper in Section 5.

1.1. Notation. In this paper, $E[\cdot]$ denotes the expectation operator; $f_X(\cdot)$ and $F_X(\cdot)$ are the probability density function (PDF) and the cumulative distribution function (CDF) of a random variable X, respectively; $\Gamma(\cdot)$ is the Gamma function; $\Pr(\cdot)$ represents the probability of a random variable; $K_v(\cdot)$ symbolizes the vth-order modified Bessel function of the second kind, and $\triangleq$ stands for the definition operator.

2. System Model

As can be seen from Figure 1, we consider a single-carrier cooperative IoT NOMA network, which consists of one source S, one AF relay R, and multiple IoT devices. In the considered system, it is infeasible to study all devices due to the extremely high complexity. Therefore, under normal circumstances, all devices are divided into multiple clusters and OMA is used for the intercluster while NOMA is utilized within clusters (In this paper, we only study the devices in the same cluster.). In one cluster, the devices are classified into two groups, namely, the far-IoT -device D_f and the near-IoT-device D_n (The near-IoT-device and the far-IoT-device are distinguished by the geographic locations of the devices away from the source node, and this case of the

two-user downlink NOMA system has been widely considered in existing works, e.g., see Ref. [34–36].). It is assumed that all nodes are equipped with a single antenna and work in the half-duplex mode. The channel coefficients and channel gains between source and relay, source and destinations, and relay and destinations are denoted as h_{SR}, h_{SD_n}, h_{SD_f}, h_{RD_f}, h_{RD_n} and ρ_{SR}, ρ_{SD_n}, ρ_{SD_f}, ρ_{RD_f}, ρ_{RD_n}, respectively. Without loss of generality, the channel gains between source and M destinations are sorted as $\rho_{SD_1} \le \rho_{SD_2} \le \cdots \le \rho_{SD_M}$.

2.1. Signal Transmission. The communication procedure is divided into two time slots. In the first time slot, S transmits signals $y_S = \sqrt{a_1 P_S} x_1 + \sqrt{a_2 P_S} x_2$ to R, D_f, and D_n, where P_S is the transmit power of S, x_1 and x_2 are the desired signals of D_f and D_n, satisfying with $E[|x_1|^2] = E[|x_2|^2] = 1$, and a_1 and a_2 are the power allocation coefficients with $a_1 + a_2 = 1$ and $a_1 > a_2$. Thus, in the first time slot, the received signals at R, D_f, and D_n can be expressed as (The subscripts S, R, D_f, and D_n in μ_t, ν_t, μ_r, and ν_r represent IQIs caused by source, relay, the far-IoT-device, and the near-IoT-device, respectively.)

$$\begin{aligned}
y_{SR} &= \mu_{r_R}\left[h_{SR}\left(\mu_{t_S} y_S + \nu_{t_S} y_S^*\right) + n_0\right] \\
&\quad + \nu_{r_R} \times \left[h_{SR}\left(\mu_{t_S} y_S + \nu_{t_S} y_S^*\right) + n_0\right]^*, \\
y_{SD_f} &= \mu_{r_{D_f}}\left[h_{SD_f}\left(\mu_{t_S} y_S + \nu_{t_S} y_S^*\right) + n_0\right] \\
&\quad + \nu_{r_{D_f}} \times \left[h_{SD_f}\left(\mu_{t_S} y_S + \nu_{t_S} y_S^*\right) + n_0\right]^*, \\
y_{SD_n} &= \mu_{r_{D_n}}\left[h_{SD_n}\left(\mu_{t_S} y_S + \nu_{t_S} y_S^*\right) + n_0\right] \\
&\quad + \nu_{r_{D_n}} \times \left[h_{SD_n}\left(\mu_{t_S} y_S + \nu_{t_S} y_S^*\right) + n_0\right]^*,
\end{aligned} \tag{1}$$

where $n_0 \sim \mathcal{CN}(0, N_0)$ denotes the additive white Gaussian noise (AWGN), μ_r, ν_r and μ_t, ν_t are the IQI coefficients caused by the RX and TX which can be expressed as

$$\begin{aligned}
\mu_t &= \frac{1}{2}(1 + \zeta_t \exp(j\phi_t)), \\
\nu_t &= \frac{1}{2}(1 - \zeta_t \exp(-j\phi_t)), \\
\mu_r &= \frac{1}{2}(1 + \zeta_r \exp(-j\phi_r)), \\
\nu_r &= \frac{1}{2}(1 - \zeta_r \exp(j\phi_r)),
\end{aligned} \tag{2}$$

where ζ_t and ζ_r are the amplitude mismatch levels caused by TX and RX, while ϕ_t and ϕ_r are the phase mismatch levels and $j = \sqrt{-1}$ denotes the unit of imaginary. Furthermore, the TX/RX image rejection ratio (IRR) is expressed as

$$\mathrm{IRR}_{t/r} = \frac{|\mu_{t/r}|^2}{|\nu_{t/r}|^2}. \tag{3}$$

According to the NOMA protocol, the received signal-to-interference-plus-noise ratio (SINR) for D_f and D_n to decoded x_1 is expressed as

$$\gamma_{SD_f} = \frac{A_f \rho_{SD_f} a_1 \gamma_1}{a_2 \rho_{SD_f} A_f \gamma_1 + \rho_{SD_f} B_f \gamma_1 + C_f}, \tag{4}$$

$$\gamma_{SD_{n\to f}} = \frac{A_n \rho_{SD_n} a_1 \gamma_1}{a_2 \rho_{SD_n} A_n \gamma_1 + \rho_{SD_n} B_n \gamma_1 + C_n}, \tag{5}$$

where $A_f = \mu_{r_{D_f}}^2 \mu_{t_S}^2 + \nu_{r_{D_f}}^2 \nu_{t_S}^2$, $A_n = \mu_{r_{D_n}}^2 \mu_{t_S}^2 + \nu_{r_{D_n}}^2 \nu_{t_S}^2$, $B_f = \mu_{r_{D_f}}^2 \nu_{t_S}^2 + \nu_{r_{D_f}}^2 \mu_{t_S}^2$, $B_n = \mu_{r_{D_n}}^2 \nu_{t_S}^2 + \nu_{r_{D_n}}^2 \mu_{t_S}^2$, $C_f = \mu_{r_{D_f}}^2 + \nu_{r_{D_f}}^2$, $C_n = \mu_{r_{D_n}}^2 + \nu_{r_{D_n}}^2$, and $\gamma_1 = P_S/N_0$ denotes the transmit SNR caused by S. Based on the ipSIC, the received SINR of D_n to decoded x_2 can be expressed as

$$\gamma_{SD_n} = \frac{a_2 A_n \rho_{SD_n} \gamma_1}{a_2 B_n \rho_{SD_n} \gamma_1 + a_1 g_{SD_n} A_n \gamma_1 + C_n}, \tag{6}$$

where $g_{SD_n} \sim \mathcal{CN}(0, \varepsilon \rho_{SD_n})$ and $\varepsilon \in (0, 1]$ is the parameter of ipSIC which follows the Gaussian distribution [37]. Note that in this system the value of ε cannot take the value of 1, because the network is completely out of the NOMA scheme when $\varepsilon = 1$, which is clearly contradictory to the considered system.

In the second time slot, the relay amplifies and forwards the received signals to the IoT devices. Thus, the received signals at D_f and D_n can be expressed as

$$\begin{aligned}
y_{RD_f} &= \mu_{r_{D_f}}\left[h_{RD_f}\left(\mu_{t_R}(Gy_{SR}) + \nu_{t_R}(Gy_{SR}^*)\right) + n_0\right] \\
&\quad + \nu_{r_{D_f}}\left[h_{RD_f}\left(\mu_{t_R}(Gy_{SR}) + \nu_{t_R}(Gy_{SR}^*)\right) + n_0\right]^*, \\
y_{RD_n} &= \mu_{r_{D_n}}\left[h_{RD_n}\left(\mu_{t_R}(Gy_{SR}) + \nu_{t_R}(Gy_{SR}^*)\right) + n_0\right] \\
&\quad + \nu_{r_{D_n}}\left[h_{RD_n}\left(\mu_{t_R}(Gy_{SR}) + \nu_{t_R}(Gy_{SR}^*)\right) + n_0\right]^*,
\end{aligned} \tag{7}$$

where $G = \sqrt{P_R/(Q(P_S \rho_{SR} + N_0))}$ represents the amplifying gain factor and P_R is the transmit power by R and $Q = (|\mu_{t_R}|^2 + |\nu_{t_R}|^2)(|\mu_{r_R}|^2 + |\nu_{r_R}|^2)$. The received SINRs for D_f to decode x_1 and for D_n to decode x_1 and x_2 are expressed as

$$\gamma_{RD_f} = \frac{a_1 E_f \rho_{SR} \rho_{RD_f} \gamma_1 \gamma_2}{(a_2 E_f + J_f)\rho_{SR} \rho_{RD_f} \gamma_1 \gamma_2 + T_f \rho_{SR} \gamma_1 + L_f \rho_{RD_f} \gamma_2 + T_f}, \tag{8}$$

$$\gamma_{RD_{n\to f}} = \frac{a_1 E_n \rho_{SR} \rho_{RD_n} \gamma_1 \gamma_2}{(a_2 E_n + J_n)\rho_{SR} \rho_{RD_n} \gamma_1 \gamma_2 + T_n \rho_{SR} \gamma_1 + L_n \rho_{RD_n} \gamma_2 + T_n}, \tag{9}$$

$$\gamma_{RD_n} = \frac{a_2 E_n \rho_{SR} \rho_{RD_n} \gamma_1 \gamma_2}{(a_2 J_n + a_1 \varepsilon E_n)\rho_{SR}\rho_{RD_n}\gamma_1\gamma_2 + L_n \rho_{RD_n}\gamma_2 + T_n \rho_{SR}\gamma_1 + T_n}, \tag{10}$$

where $\gamma_1 = P_R/N_0$ represents the transmit SNR caused by R, $E_f = (\mu_{r_R}^2\mu_{t_S}^2 + \nu_{r_R}^2\nu_{t_S}^2)(\mu_{r_{D_f}}^2\mu_{t_R}^2 + \nu_{r_{D_f}}^2\nu_{t_R}^2) + (\mu_{r_R}^2\nu_{t_S}^2 + \mu_{t_S}^2\nu_{r_R}^2)(\mu_{r_{D_f}}^2\nu_{t_R}^2 + \mu_{t_R}^2\nu_{r_{D_f}}^2)$, $E_n = (\mu_{r_R}^2\mu_{t_S}^2 + \nu_{r_R}^2\nu_{t_S}^2)(\mu_{r_{D_n}}^2\mu_{t_R}^2 + \nu_{r_{D_n}}^2\nu_{t_R}^2) + (\mu_{r_R}^2\nu_{t_S}^2 + \mu_{t_S}^2\nu_{r_R}^2)(\mu_{r_{D_n}}^2\nu_{t_R}^2 + \mu_{t_R}^2\nu_{r_{D_n}}^2)$, $J_f = (\mu_{r_R}^2\nu_{t_S}^2 + \mu_{t_S}^2 \times \nu_{r_R}^2)(\mu_{r_{D_f}}^2\mu_{t_R}^2 + \nu_{r_{D_f}}^2\nu_{t_R}^2) + (\mu_{r_{D_f}}^2\nu_{t_R}^2 + \mu_{t_R}^2\nu_{r_{D_f}}^2)(\mu_{r_R}^2\mu_{t_S}^2 + \nu_{r_R}^2\nu_{t_S}^2)$, $J_n = (\mu_{r_R}^2\nu_{t_S}^2 + \mu_{t_S}^2\nu_{r_R}^2)(\mu_{r_{D_n}}^2\mu_{t_R}^2 + \nu_{r_{D_n}}^2 \times \nu_{t_R}^2) + (\mu_{r_{D_n}}^2\nu_{t_R}^2 + \mu_{t_R}^2\nu_{r_{D_n}}^2)(\mu_{r_R}^2\mu_{t_S}^2 + \nu_{r_R}^2\nu_{t_S}^2)$, $L_f = 2\mu_{r_{D_f}}^2\mu_{t_R}^2 + 2\mu_{r_{D_f}}^2\nu_{t_R}^2 + 2\nu_{r_{D_f}}^2\mu_{t_R}^2 + 2\nu_{r_{D_f}}^2\nu_{t_R}^2$, $L_n = 2\mu_{r_{D_n}}^2\mu_{t_R}^2 + 2\mu_{r_{D_n}}^2\nu_{t_R}^2 + 2\nu_{r_{D_n}}^2\mu_{t_R}^2 + 2\nu_{r_{D_n}}^2\nu_{t_R}^2$, $T_f = QC_f$, and $T_f = C_nQ$.

2.2. Fading Channels. Assume that all the channel gains follow Nakagami-m distribution; thus, the PDF and CDF of ρ_i can be expressed as [38]

$$f_{\rho_i}(x) = \frac{x^{\alpha_i - 1}}{\Gamma(\alpha_i)\beta_i^{\alpha_i}} e^{-x/\beta_i}, \tag{11}$$

$$F_{\rho_i}(x) = 1 - \sum_{g_i=0}^{\alpha_i - 1} \frac{e^{-x/\beta_i}}{g_i!}\left(\frac{x}{\beta_i}\right)^{g_i}, \tag{12}$$

where α_i denotes the multipath fading parameter while β_i represents the control spread parameter. By utilizing the order statistics, the PDF and CDF of the m-th devices' channel gain ρ_m can be expressed as

$$f_{\rho_m}(x) = \frac{M!}{(m-1)!(M-m)!}\left[F_{\rho_i}(x)\right]^{m-1} \times f_{\rho_i}(x)\left[1 - F_{\rho_i}(x)\right]^{M-m}, \tag{13}$$

$$F_{\rho_m}(x) = \frac{M!}{(m-1)!(M-m)!}\sum_{z=0}^{M-m}\binom{M-m}{z} \times \frac{(-1)^z}{m+z}\left[F_{\rho_i}(x)\right]^{m+z}, \tag{14}$$

where M denotes the total numbers of IoT devices.

3. Outage Probability Analysis

In this section, the outage performances of D_f and D_n are discussed. We first analyze the considered system by deriving the exact expressions of the outage probability and then formulate the asymptotic analysis in the high SNR. In addition, the throughput of the considered system is also explored.

3.1. Exact Outage Probability. For D_f, the outage event will occur when D_f fails to decode the expected signal x_1 transmitted from S and R. Therefore, the outage probability of D_f can be expressed as

$$P_{\text{out}}^{D_f} = \Pr\left(\gamma_{SD_f} < \gamma_{thf}\right)\Pr\left(\gamma_{RD_f} < \gamma_{thf}\right), \tag{15}$$

where γ_{thf} is the target threshold at D_f. The closed-form expression of outage probability of D_f under IQI and ipSIC is provided in the following theorem.

Theorem 1. *The exact outage probability expression of D_f in the presence of IQI and ipSIC is expressed as*

$$\begin{aligned} P_{out}^{D_f} = {} & b_f \sum_{z=0}^{M-f}\binom{M-f}{z}\frac{(-1)^z}{f+z} \\ & \cdot \left[1 - e^{-\theta/\beta_{SD_f}}\sum_{g_5=0}^{\alpha_{SD_f}-1}\frac{1}{g_5}\times\left(\frac{\theta}{\beta_{SD_f}}\right)^{g_5}\right]^{f+z} \\ & \cdot \left[1 - \frac{2}{\Gamma\left(\alpha_{RD_f}\right)\beta_{RD_f}^{\alpha_{RD_f}}}\sum_{g_1=0}^{\alpha_{SR}-1}\sum_{t_1=0}^{\alpha_{RD_f}-1}\sum_{t_2=0}^{g_1}\frac{1}{g_1!}\right. \\ & \times \binom{g_1}{g_2}\binom{\alpha_{RD_f}-1}{t_1} \\ & \cdot \left(\beta_{SR}\gamma_1 T_f\right)^{-g_1-(t_1-t_2+1/2)}\varphi^{g_1+\alpha_{RD_f}-(t_1+t_2+1/2)} \\ & \times \left(T_f + L_f\gamma_2\varphi\right)^{((t_1+t_2+1)/2)}\beta_{RD_f}^{(t_1-t_2+1)/2}\left(L_f\gamma_2\right)^{g_1-t_2} \\ & \left. \times e^{-\left(\varphi/\beta_{RD_f}\right)-\left(L_f\gamma_2\varphi/\beta_{SR}T_f\gamma_1\right)} \right. \\ & \left. \cdot K_{t_1-t_2+1}\left(2\sqrt{\frac{\left(T_f + L_f\gamma_2\varphi\right)\varphi}{\beta_{SR}\beta_{RD_f}T_f\gamma_1}}\right)\right], \end{aligned} \tag{16}$$

where f denotes the f-th device (the far device), $b_f \triangleq M!/(f-1)!(M-f)!$, $\theta \triangleq C_f\gamma_{thf}/[a_1A_f\gamma_1 - (a_1A_f + B_f)\gamma_1\gamma_{thf}]$ with $A_fa_1 > (a_1A_f + B_f)\gamma_{thf}$, and $\varphi \triangleq T_f\gamma_{thf}/[a_1E_f\gamma_2 - (a_2E_f + J_f)\gamma_2\gamma_{thf}]$ with $a_1E_f > (a_2E_f + J_f)\gamma_{thf}$.

Proof. See Appendix A.

For D_n, the outage event will occur when D_n fails to decode either the signals x_1 or x_2 transmitted from S or R. Therefore, the outage probability of D_n can be expressed as

$$P_{\text{out}}^{D_n} = \left[1 - \Pr\left(\gamma_{SD_{n\to f}} > \gamma_{thf}, \gamma_{SD_n} > \gamma_{thn}\right)\right]s \times \left[1 - \Pr\left(\gamma_{RD_{n\to f}} > \gamma_{thf}, \gamma_{RD_n} > \gamma_{thn}\right)\right], \tag{17}$$

where γ_{thn} is the target threshold at D_n. The closed-form expression of outage probability of D_n under IQI and ipSIC is provided in the following theorem.

Theorem 2. *The exact outage probability expression of D_n in the presence of IQI and ipSIC is expressed as*

$$P_{out}^{D_n} = b_n \sum_{z=0}^{M-n} \binom{M-n}{z} \frac{(-1)^z}{n+z} \cdot \left[1 - \sum_{g_4=0}^{\alpha_{SD_n}-1} \frac{1}{g_4!} e^{-\xi/\beta_{SD_n}} \times \left(\frac{\xi}{\beta_{SD_n}}\right)^{g_4}\right]^{n+z} \cdot \left[1 - \frac{2}{\alpha_{RD_n}\beta_{RD_n}^{\alpha_{RD_n}}} \sum_{g_1=0}^{\alpha_{SR}-1} \sum_{q_1=0}^{\alpha_{RD_n}-1} \sum_{q_2=0}^{g_1} \frac{1}{g_1!} \times \binom{g_1}{q_2} \binom{\alpha_{RD_n}-1}{q_1} \cdot (\beta_{SR}\gamma_1 T_n)^{-g_1-((q_1-q_2+1)/2)} \tau^{g_1+\alpha_{RD_n}-((q_1+q_2+1)/2)} \times (T_n + L_n\gamma_2\tau)^{(q_1+q_2+1)/2} \beta_{RD_n}^{(q_1-q_2+1)/2} (L_n\gamma_2)^{g_1-q_2} \times e^{-\left(\tau/\beta_{RD_n}\right)-(L_n\gamma_2\tau/\beta_{SR}T_n\gamma_1)} \cdot K_{q_1-q_2+1}\left(2\sqrt{\frac{(T_n+L_n\gamma_2\tau)\tau}{\beta_{SR}\beta_{RD_n}T_f\gamma_1}}\right)\right], \tag{18}$$

where n denotes the n-th device (the near device) and $b_n \triangleq M!/(n-1)!(M-n)!$, $\xi \triangleq \max(\xi_1, \xi_2)$, $\xi_1 \triangleq C_f\gamma_{thf}/[a_1A_n\gamma_1 - (a_1A_n + B_n)\gamma_1\gamma_{thf}]$, $\xi_2 \triangleq C_n\gamma_{thn}/[a_2A_n\gamma_1 - \gamma_1\gamma_{thn}(a_2B_n + a_1\varepsilon A_n)]B_n + a_1\varepsilon A_n)]$, $\tau = \max(\tau_1, \tau_2)$, $\tau_1 \triangleq T_n\gamma_1\gamma_{thf}/[a_1E_n\gamma_2 - (a_2E_n + J_n)\gamma_2\gamma_{thf}]$, and $\tau_2 \triangleq T_n\gamma_{thn}/[a_2E_n\gamma_2 - (a_2J_n + a_1\varepsilon E_n)\gamma_2\gamma_{thn}]$.

Proof. See Appendix B.

Remark 3. From Theorems 1 and 2, we can observe that the outage probabilities of D_f and D_n are determined by IQI parameters, the performance of SIC, fading parameters, and distortion noise. Meanwhile, it is worth noting that when $\varsigma_t = \varsigma_r = 1$, $\phi_t = \phi_r = 0°$, and $\varepsilon = 0$ are all satisfied, the considered system reduces to ideal conditions.

3.2. Asymptotic Outage Probability. In this subsection, the asymptotic outage probabilities of D_f and D_n are analyzed to obtain more insights on the outage behavior of the considered system. The asymptotic CDF of the channel gain ρ_i in the case of ordering and nonordering can be expressed as [39]

$$f_{\rho_i}^{\infty}(x) = \frac{x^{\alpha_i}}{\alpha_i!\beta_i^{\alpha_i}}, \tag{19}$$

$$F_{\rho_i}^{\infty}(x) = \frac{M!}{(M-m)!m!} \left(\frac{1}{\alpha_i}\right)^m \left(\frac{x}{\beta_i}\right)^{m\alpha_i}. \tag{20}$$

The asymptotic expressions of outage probabilities of D_f and D_n are described in the following corollaries.

Corollary 4. *The asymptotic closed form of outage probability of D_f in the high SNR regime is expressed as*

$$P_{out}^{D_f,\infty} = b_f^{\infty} \left(\frac{1}{\alpha_{SD_f}!}\right)^f \left(\frac{\theta}{\beta_{SD_f}}\right)^{\alpha_{SD_f}f} \times \left(\frac{\varphi'^{\alpha_{SR}}}{\alpha_{SR}!\beta_{SR}^{\alpha_{SR}}} + \frac{\varphi''^{\alpha_{RD_f}}}{\alpha_{RD_f}!\beta_{RD_f}^{\alpha_{RD_f}}}\right), \tag{21}$$

where $b_f^{\infty} = M!/[f!(M-f)!]$, $\varphi' = L_f\gamma_{thf}/[a_1E_f\gamma_1 - (a_2E_f + J_f)\gamma_1\gamma_{thf}]E_f\gamma_1 - (a_2E_f + J_f)\gamma_1\gamma_{thf}]$, and $\varphi'' = T_f\gamma_{thf}/[a_1\gamma_2E_f - (a_2E_f + J_f)\gamma_2\gamma_{thf}]$.

Proof. See Appendix C.

Corollary 5. *The asymptotic closed form of outage probability of D_n in the high SNR regime is expressed as*

$$P_{out}^{D_n,\infty} = b_n^{\infty} \left(\frac{1}{\alpha_{RD_n}!}\right)^n \left(\frac{\xi}{\beta_{RD_n}}\right)^{n\alpha_{SD_n}} \times \left(\frac{\tau'^{\alpha_{SR}}}{\alpha_{SR}!\beta_{SR}^{\alpha_{SR}}} + \frac{\tau''^{\alpha_{RD_n}}}{\alpha_{RD_n}!\beta_{RD_n}^{\alpha_{RD_n}}}\right), \tag{22}$$

where $b_n^{\infty} = M!/[n!(M-n)!]$, $\tau' = \max(\tau_1', \tau_2')$, $\tau'' = \max(\tau_1'', \tau_2'')$, $\tau_1' \triangleq L_n\gamma_{thf}/[a_1E_n\gamma_1 - \gamma_1\gamma_{thf}(a_2E_n + J_n)]$, $\tau_1'' \triangleq T_n\gamma_{thf}/[a_1E_n\gamma_2 - \gamma_2\gamma_{thf}(a_2E_n + J_n)]$, $\tau_2' \triangleq L_n\gamma_{thn}/[a_2E_n\gamma_1 - a_2J_n\gamma_{thn}\gamma_1]$, and $\tau_2'' \triangleq T_n\gamma_{thn}/[a_2E_n\gamma_2 - a_2J_n\gamma_{thn}\gamma_2]$.

Proof. See Appendix D.

Remark 6. The results of Corollaries 4 and 5 show the effects of channel fading parameters, IQI parameters, the performance of SIC, and distortion noise on asymptotic outage performances of D_f and D_n. In addition, we can also observe that the asymptotic outage probability is related to the order of user arrangement directly.

3.3. Diversity Order. The diversity order can reflect the trend of the outage probability intuitively. To this end, the diversity order of the considered system is explored in this subsection. The diversity order is defined as [40]

$$d = -\lim_{\gamma\to\infty} \frac{\log\left(P_{\text{out}}^{D_{m,\infty}}\right)}{\log\gamma}, \tag{23}$$

where $P_{\text{out}}^{D_{m,\infty}}$ denotes asymptotic outage probability of m-th device and $\gamma \in [\gamma_1, \gamma_2]$ represents the transmitted SNR.

Corollary 7. *Based on (23), the diversity orders of D_f and D_n in ideal conditions ($\varsigma_t = \varsigma_r = 1$, $\phi_t = \phi_r = 0°$, and $\varepsilon = 0$) and*

nonideal conditions ($\varsigma_t, \varsigma_r \neq 1$, $\phi_t, \phi_r \neq 0^\circ$, *and* $\varepsilon \neq 0$) *can be written as*

$$d_f^{id} = d_f^{nid} = \min\left(f\alpha_{SD_f}\alpha_{SR}, f\alpha_{SD_f}\alpha_{RD_f}\right),$$
$$d_n^{id} = d_n^{nid} = \min\left(n\alpha_{SD_n}\alpha_{SR}, n\alpha_{SD_n}\alpha_{RD_n}\right). \quad (24)$$

Remark 8. The results show that the diversity order of D_f is the minimum of $f\alpha_{SD_f}\alpha_{SR}$ and $f\alpha_{SD_f}\alpha_{RD_f}$, which indicates that the diversity order of D_f is relative to α_{SD_f}, α_{SR}, α_{RD_f}, and f, while the value is affected by the multipath fading parameters α_{SR} and α_{RD_f} of $S \longrightarrow R$ and $R \longrightarrow D_f$. Similarly, the diversity order of D_n is the minimum of $n\alpha_{SD_n}\alpha_{SR}$ and $n\alpha_{SD_n}\alpha_{RD_n}$, which is related to α_{SD_n}, α_{SR}, α_{RD_n}, and n, and the final value is jointly determined by α_{SR} and α_{RD_n}. The results also show that the outage probabilities of D_f and D_n of the considered system will always decrease with the increase of SNR. In addition, we can also observe that although the outage probabilities of IoT devices in ideal and nonideal conditions are different, the trends are the same due to the diversity orders.

3.4. Throughput Analysis. The system throughput is another measure of system performance, which is the number of signals transmitted per unit of time successfully. Thus, the system throughput is formulated as [41]

$$T = \sum_{m=1}^{M}\left(1 - P_{\text{out}}^{D_m}\right)R_{thm}, \quad (25)$$

where $P_{\text{out}}^{D_m}$ is the outage probability of D_m which can be obtained from (16) and (18), $R_{thm} = (1/2)\log(1+\gamma_{thm})$ denotes the target rate of D_m, and 1/2 represents that the communication transmit process is divided into two time slots.

3.5. Energy Efficiency. To further evaluate the performance of the considered system, the energy efficiency is analyzed in this subsection. Energy efficiency refers to the useful signals that IoT devices received for each unit of energy consumed by S. Hence, the energy efficiency of the considered system can be expressed as [42]

$$\eta_{ee} = \frac{T}{P_{EE}}, \quad (26)$$

where $P_{EE} = P_S + P_R + P_C$ denotes total energy consumption and P_C is the fixed energy consumption which is caused by transmitter and the IoT devices and T is the system throughput which can be obtained from (25).

4. Numerical Results

In this section, the correctness of analytical results in Section 3 is demonstrated by some computer simulations. Unless otherwise noted, the simulation parameters are provided in Table 1.

Table 1: Simulation parameters.

Parameters	Value	Parameters	Value
α_i	2	β_i	1
n	2	f	1
γ_{thf}	1.5	γ_{thn}	3
M	2	N_0	1
P_C	0.1 W		

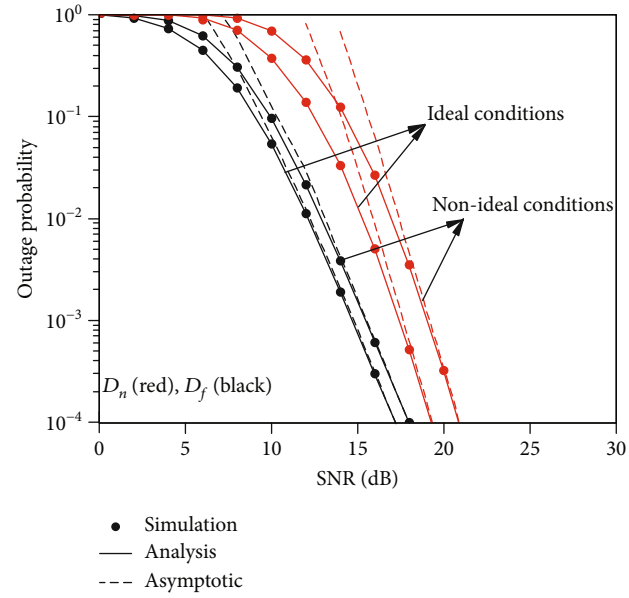

Figure 2: Outage probability of IoT devices versus transmit SNR in different conditions.

Figure 2 shows the outage probabilities of IoT devices versus transmit SNR in ideal conditions ($\varsigma_t = \varsigma_r = 1$, $\phi_t = \phi_r = 0^\circ$, and $\varepsilon = 0$) and nonideal conditions ($\varsigma_t = \varsigma_r = 1.2$, $\phi_t = \phi_r = 10^\circ$, and $\varepsilon = 0.01$) with $a_1 = 0.8$ and $a_2 = 0.2$. The perfect coincidence of the theoretical analysis value and the Monte Carlo simulation value curves in Figure 2 verifies our derivations in (16), (18), (21), and (22). From Figure 2, we can observe that the gaps caused by ideal and nonideal conditions of D_n are larger than those of D_f. The reason for this phenomenon can be explained by the fact that ipSIC has no impact on D_f. As can also be seen from Figure 2, the curves of different IoT devices are almost parallel in the high SNR region. Meanwhile, we also notice that the outage probability of the far-IoT-device outperforms that of the near-IoT-device, because of the large power allocation factor. Additionally, the results also show that the outage performance of the considered system can be greatly prompted by improving the transmitting SNR.

Figure 3 illustrates the outage probabilities of the IoT devices versus IRR in perfect I/Q and IQI conditions with $\text{IRR}_t = \text{IRR}_r$, SNR = 15 dB, $\varepsilon = 0.01$, and $a_1 = 0.8$ and $a_2 = 0.2$ for power allocation. As can be seen from Figure 3, with the increase of IRR, the outage performances of devices D_f and D_n improve continuously, and when IRR > 32 dB, the

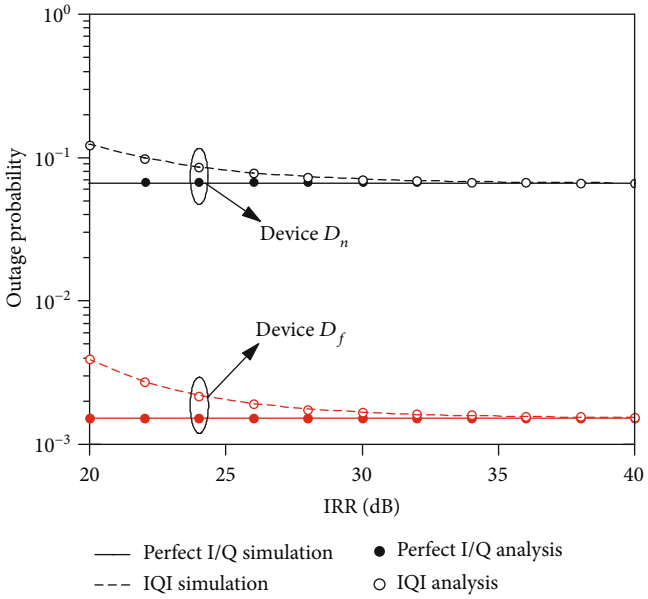

Figure 3: Outage probability of IoT devices versus IRR in different conditions.

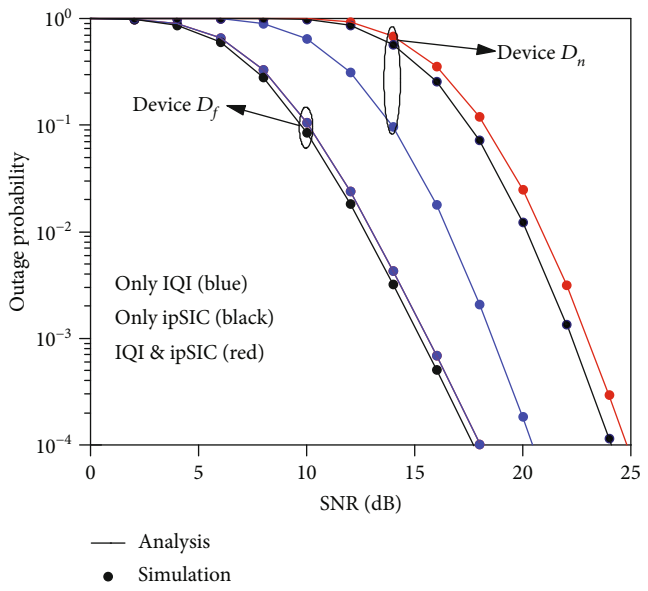

Figure 4: Outage probability of IoT devices versus SNR under different nonideal factors.

outage probabilities of the devices almost coincide with those of the ideal IQ matching. In addition, in terms of the gaps between the perfect IQ matching and IQI curves in the figure, IQI has different effects on the outage performances of different IoT devices in the considered NOMA system. Furthermore, we can also observe that the outage performance of the far-IoT-device is better than that of the near device, which is due to the more power allocation obtained by the far device.

Figure 4 plots the variations of outage probabilities of the IoT devices with the increase of SNR in the presence of different nonideal factors with $a_1 = 0.8$ and $a_2 = 0.2$. In the simulation, we assume three cases: (1) only IQI ($\varsigma_t = \varsigma_r \neq 1.05$, $\phi_t = \phi_r \neq 9°$, and $\varepsilon = 0$), (2) only ipSIC ($\varsigma_t = \varsigma_r = 1$, $\phi_t = \phi_r = 0°$, and $\varepsilon = 0.05$), and (3) both IQI and ipSIC ($\varsigma_t = \varsigma_r = 1.05$, $\varepsilon = 0.05$, and $\phi_t = \phi_r = 9°$). The reason for setting the nonideal factors in this way is to ensure that the level of IQ mismatch is at the same extent as the level of ipSIC. For the near-IoT-device D_n, the case of only IQI outperforms the case of only ipSIC in the outage performance which indicates that ipSIC has a severe negative impact on the considered system. Interestingly, the curves of only IQI and both ipSIC and IQI are coincident, since in the NOMA system, the outage performance of D_f is not affected by SIC.

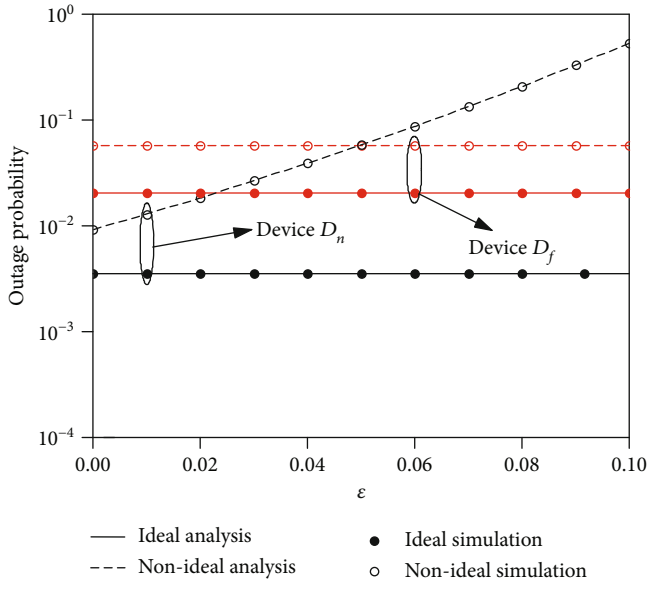

Figure 5: Outage probability of IoT devices versus ε in different conditions.

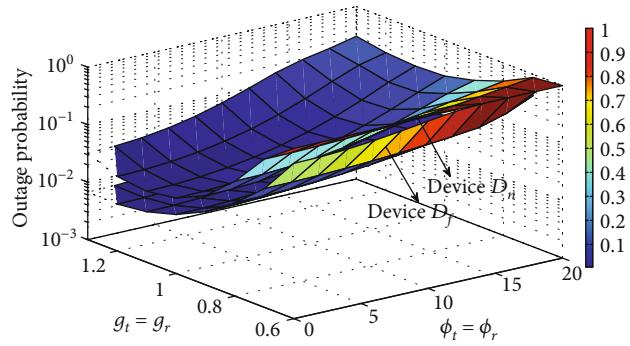

Figure 6: Outage probability of IoT devices versus g and ϕ.

As a further development, Figure 5 presents the outage performances of IoT devices versus ε with SNR = 15 dB. For nonideal conditions, we set $\varsigma_t = \varsigma_r = 1.2$ and $\phi_t = \phi_r = 10°$. It can be observed from Figure 5 that, for the far-IoT-device D_f, the outage probabilities in either ideal or nonideal conditions will not change with the variation of ε, which is due to the fact that the outage performance of D_f is independent of the performance of SIC, while for D_n the outage probability almost increases linearly with the increase of ε. This indicates

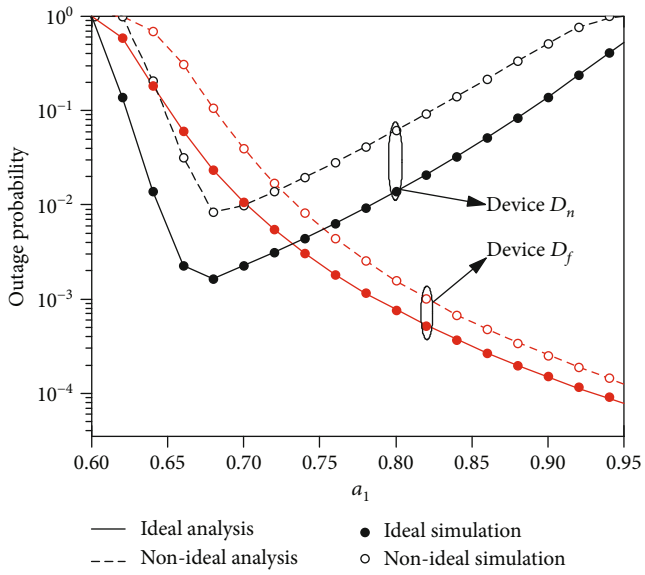

FIGURE 7: Outage probability of IoT devices versus a_1 in different conditions.

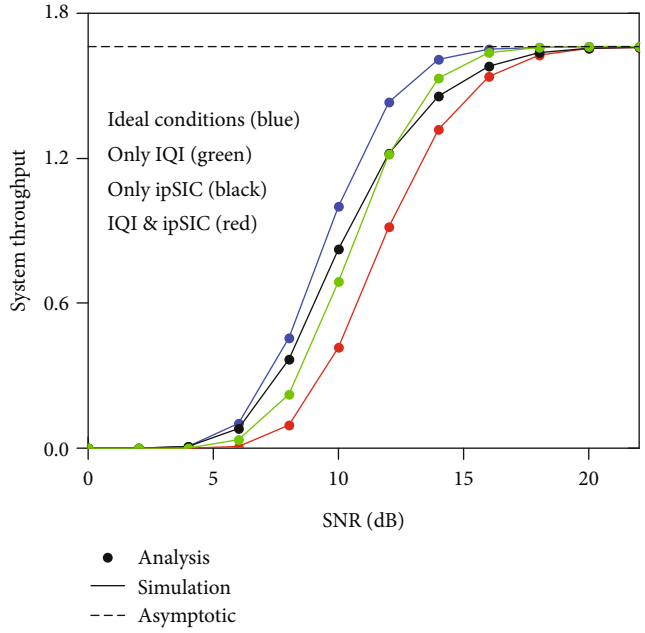

FIGURE 8: System throughput versus SNR in different conditions.

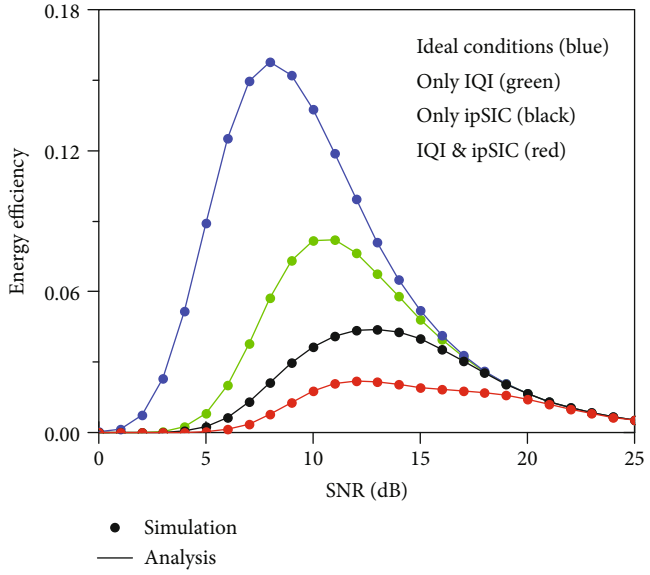

FIGURE 9: Energy efficiency versus SNR under different nonideal factors.

that SIC is vital in the outage performance of D_n. From Figure 5, we can also see that when $\varepsilon = 0$, there are gaps between the outage probabilities of ideal and nonideal conditions, which is due to the existence of IQI in the considered system. It is worth noting that although we have mentioned $\varepsilon \in [0, 1)$ in Section 2, the maximum value of ε here is taken as 0.1. The reason is that $a_2 A_n > (a_2 B_n + a_1 \varepsilon A_n)\gamma_{thn}$ and $a_2 E_n > (a_2 J_n + a_1 \varepsilon E_n)\gamma_{thn}$ are all needed to be satisfied from (18). Thus, when $\varepsilon = 0.1$, the outage probability of D_n is almost 1.

Figure 6 analyzes the impact of amplitude and phase mismatch levels on the outage probabilities versus SNR for different IoT devices with SNR = 15 dB, $\varepsilon = 0.01$, and $a_1 = 0.7$ and $a_2 = 0.3$ for power allocation. For simplicity, in this simulation, we set $g_{t_S} = g_{t_R} = g_{r_R} = g_{r_D}$ and $\phi_{t_S} = \phi_{t_R} = \phi_{r_R} = \phi_{r_D}$. As can be seen from Figure 6, when $0.6 < g < 1$, the outage probabilities decrease with the increase of g; however, when $1 < g < 1.3$, the opposite phenomenon appears. This can be explained that when the amplitude mismatch levels are closer to 1, the system is closer to the ideal conditions. Another observation is that the outage performances of IoT devices deteriorate with the increase of ϕ, and when the phase mismatch levels reach to about 20°, the considered system turns meaningless due to the high outage probability.

Figure 7 investigates the outage probabilities of IoT devices versus power allocation a_1 with SNR = 15 dB in ideal conditions and nonideal conditions for $\varsigma_t = \varsigma_r = 1.2$, $\phi_t = \phi_r = 10°$, and $\varepsilon = 0.01$. The outage probability of D_n first decreases and then increases with the increase of a_1, and when a_1 is about 0.68, the outage probability of D_n reaches the minimum. This can be deciphered that when $0.5 < a_1 < 0.6$, the considered network is always in an off-line state due to the insufficient power level for D_f, and when $0.6 < a_1 < 0.68$, the considered system begins to perform NOMA; after that, the outage performance of D_n begins to deteriorate as the power allocation to D_n decreases. Unlike D_n, the outage probability of D_f keeps decreasing as the power allocated to it increases.

Figure 8 shows the exact and asymptotic system throughput versus SNR. In this simulation, we set $\varsigma_t = \varsigma_r = 1.3$, $\phi_t = \phi_r = 15°$, and $\varepsilon = 0.05$ for nonideal factors and $a_1 = 0.7$ and $a_2 = 0.3$ for power allocation. When the SNR is lower than 5 dB, the throughput of the considered system is almost 0 due to the high outage probability. And the system throughput tends to be a fixed value in the high SNR regime. This is because when the SNR is large enough, the outage probabilities of IoT devices are almost close to 0. It is worth

mentioning that there exists an intersection between the green curve (only IQI in the considered system) and the black curve (only ipSIC in the considered system), which indicates that in the case of low SNR, IQI has a greater impact on the system throughput, while ipSIC will have a more severe impact on the considered system in the moderate and high SNR region. From Figure 8, we can also find that these nonideal factors play a negative role in the considered system.

In Figure 9, the energy efficiency of the considered system versus SNR is plotted. From the figure, we can see that in both ideal and nonideal conditions, the energy efficiency of the considered system first increases and then decreases, which is due to the fact that when the SNR is low, most of the transmission power is used for signal transmission. From the figure, we can also observe that the energy efficiency of the system which is only affected by IQI is higher than that only affected by ipSIC. This indicates that compared with IQI, the energy efficiency of the considered system is more dependent on the performance of SIC. In addition, we can also observe that when SNR > 20 dB, the energy efficiencies of the considered system in the four cases are almost identical. Finally, we can also conclude that the overall performance of the system cannot be improved by simply increasing the SNR in practical communication networks.

5. Conclusion

In this paper, the performance of cooperative AF IoT NOMA system in the presence of IQI and ipSIC is studied. The exact and asymptotic outage probability expressions are derived to evaluate the considered system. Furthermore, the diversity order in the high SNR region, the system throughput, and the energy efficiency are also presented. The results show that IQI and ipSIC play negative roles in the considered system performance and the outage performance of the considered system will be greatly improved with the increase of SNR. Compared with IQI, identical degree of ipSIC plays a greater impact on the outage performance. Particularly, tuning the power allocation scheme properly can improve the outage performances of the IoT devices. The results also show that, according to the inherent characteristics of the NOMA scheme, the outage probability of the far-IoT-device is independent of the SIC performance. In addition, the simulation results of the system throughput and the energy efficiency show that the system performance cannot be improved by simply improving the SNR.

Appendix

A. Proof of Theorem 1

By substituting (4) and (8) into (15), the outage probability of D_f is rewritten as

$$P_{\text{out}}^{D_f} = \underbrace{\Pr\left(\frac{a_1 A_f \rho_{SD_f}\gamma_1}{a_2\rho_{SD_f}A_f\gamma_1 + \rho_{SD_f}B_f\gamma_1 + C_f} < \gamma_{thf}\right)}_{I_1} \times \underbrace{\Pr\left(\frac{a_1 E_f \rho_{SR}\rho_{RD_f}\gamma_1\gamma_2}{\left(a_2E_f + J_f\right)\rho_{SR}\rho_{RD_f}\gamma_1\gamma_2 + T_f\rho_{SR}\gamma_1 + L_f\rho_{RD_f}\gamma_2 + T_f} < \gamma_{thf}\right)}_{I_2}. \tag{A.1}$$

Utilizing the PDF and CDF in (11)–(14), I_1 and I_2 can be further expressed as

$$I_1 = \Pr\left(\rho_{SD_f} < \theta\right) = b_f \sum_{z=0}^{M-f}\binom{M-f}{z}\frac{(-1)^z}{f+z} \cdot \left[1 - \sum_{g_5=0}^{\alpha_{SD_f}-1}\frac{1}{g_5}e^{-\theta/\beta_{SD_f}}\left(\frac{\theta}{\beta_{SD_f}}\right)^{g_5}\right]^{f+z}, \tag{A.2}$$

$$\begin{aligned} I_2 &= 1 - \Pr\left(\rho_{RD_f} > \varphi, \rho_{SR} > \frac{\left(T_f + L_f\gamma_2\rho_2\right)\varphi}{\left(\rho_2 - \varphi\right)T_f\gamma_1}\right) \\ &= \int_{\varphi}^{\infty} f_{\rho_{RD_f}}(y)dy \int_{\left(T_f + L_f\gamma_2\rho_2\right)\varphi/(y-\varphi)T_f\gamma_1}^{\infty} f_{\rho_{SR}}(x)dx \\ &= 1 - \frac{2}{\Gamma\left(\alpha_{RD_f}\right)\beta_{RD_f}^{\alpha_{RD_f}}}\sum_{g_1=0}^{\alpha_{SR}-1}\sum_{t_1=0}^{\alpha_{RD_f}-1}\sum_{t_2=0}^{g_1}\frac{1}{g_1!}\binom{\alpha_{RD_f}-1}{t_1} \\ &\quad \times \binom{g_1}{g_2}\left(\frac{1}{\beta_{SR}\gamma_1 T_f}\right)^{g_1+((t_1-t_2+1)/2)} \\ &\quad \cdot \varphi^{g_1+\alpha_{RD_f}-(t_1+t_2+1)/2}\left(L_f\gamma_2\right)^{g_1-t_2} \\ &\quad \times \left(T_f + L_f\gamma_2\varphi\right)^{(t_1+t_2+1)/2}\beta_{RD_f}^{(t_1-t_2+1)/2}e^{-\left(\varphi/\beta_{RD_f}\right)-\left(L_f\gamma_2\varphi/\beta_{SR}T_f\gamma_1\right)} \\ &\quad \times K_{t_1-t_2+1}\left(2\sqrt{\frac{\left(T_f + L_f\gamma_2\varphi\right)\varphi}{\beta_{SR}\beta_{RD_f}T_f\gamma_1}}\right). \end{aligned} \tag{A.3}$$

Combining (A.2) and (A.3) with (A.1), the outage probability of D_f can be obtained.

B. Proof of Theorem 2

By substituting (5), (6), (9), and (10) into (17), the outage probability of D_n is rewritten as

$$P_{\text{out}}^{D_f} = \left[1 - \Pr\left(\gamma_{SD_{n\to f}} > \gamma_{thf}, \gamma_{SD_n} > \gamma_{thn}\right)\right]\left[1 - \Pr\left(\gamma_{RD_{n\to f}} > \gamma_{thf}, \gamma_{RD_n} > \gamma_{thn}\right)\right]$$
$$= \underbrace{\left[1 - \Pr\left(\frac{A_n\rho_{SD_n}a_1\gamma_1}{(a_2A_n + B_n)\rho_{SD_n}\gamma_1 + C_n} > \gamma_{thf}, \frac{a_2A_n\rho_{SD_n}\gamma_1}{(a_2B_n + a_1\varepsilon A_n)\rho_{SD_n}\gamma_1 + C_n} > \gamma_{thn}\right)\right]}_{I_3}$$
$$\times \underbrace{\left[1 - \Pr\left(\frac{a_1E_n\rho_{SR}\rho_{RD_n}\gamma_1\gamma_2}{(a_2E_n + J_n)\rho_{SR}\rho_{RD_n}\gamma_1\gamma_2 + T_n\rho_{SR}\gamma_1 + L_n\rho_{RD_n}\gamma_2 + T_n} > \gamma_{thf}, \frac{a_2E_n\rho_{SR}\rho_{RD_n}\gamma_1\gamma_2}{(a_2J_n + a_1\varepsilon E_n)\rho_{SR}\rho_{RD_n}\gamma_1\gamma_2 + L_n\rho_{RD_n}\gamma_2 + T_n\rho_{SR}\gamma_1 + T_n} > \gamma_{thn}\right)\right]}_{I_4}. \tag{B.1}$$

Utilizing the PDF and CDF in (11)–(14), I_3 and I_4 can be further expressed as

$$I_3 = 1 - \Pr\left(\rho_{SD_n} < \xi\right) = b_n\sum_{z=0}^{M-n}\binom{M-n}{z}\frac{(-1)^z}{n+z} \cdot \left[1 - \sum_{g_4=0}^{\alpha_{SD_n}-1}\frac{1}{g_4!}e^{-\xi/\beta_{SD_n}}\left(\frac{\xi}{\beta_{SD_n}}\right)^{g_4}\right]^{n+z}, \tag{B.2}$$

$$I_4 = 1 - \Pr\left(\rho_{RD_n} > \tau, \rho_{SR} > \frac{\left(T_n + L_n\gamma_2\rho_{RD_n}\right)\tau}{\left(\rho_{RD_n} - \tau\right)T_n\gamma_1}\right)$$
$$= \int_\tau^\infty f_{\rho_{RD_n}}(y)dy\int_{(T_n+L_n\gamma_2 y)\tau/(y-\tau)T_n\gamma}^\infty f_{\rho_{SR}}(x)dx$$
$$= 1 - \frac{2}{\alpha_{RD_n}\beta_{RD_n}^{\alpha_{RD_n}}}\sum_{g_1=0}^{\alpha_{SR}-1}\sum_{q_1=0}^{\alpha_{RD_n}-1}\sum_{q_2=0}^{g_1}\frac{1}{g_1!}\binom{\alpha_{RD_n}-1}{q_1}\binom{g_1}{q_2}$$
$$\times\left(\frac{1}{\beta_{SR}\gamma_1T_n}\right)^{g_1+(q_1-q_2+1)/2}\tau^{g_1+\alpha_{RD_n}-(q_1+q_2+1)/2}\beta_{RD_n}^{(q_1-q_2+1)/2}$$
$$\times\left(T_n + L_n\gamma_2\tau\right)^{(q_1+q_2+1)/2}\left(L_n\gamma_2\right)^{g_1-q_2}e^{-\left(\tau/\beta_{RD_n}\right)-\left(L_n\gamma_2\tau/\beta_{SR}T_n\gamma_1\right)}$$
$$\times K_{q_1-q_2+1}\left(2\sqrt{\frac{(T_n + L_n\gamma_2\tau)\tau}{\beta_{SR}\beta_{RD_n}T_f\gamma_1}}\right). \tag{B.3}$$

Combining (B.2) and (B.3) with (B.1), the outage probability of D_n can be obtained.

C. Proof of Corollary 1

Based on (A.1), the asymptotic outage probability of D_f can be expressed as

$$P_{\text{out}}^{D_f,\infty} = I_1^\infty I_2^\infty. \tag{C.1}$$

Utilizing the asymptotic CDF in (19), I_1^∞ can be further expressed as

$$I_1^\infty = \Pr\left(\rho_{SD_n} < \theta\right) \approx b_f^\infty\left(\frac{1}{\alpha_{SD_f}!}\right)^f\left(\frac{\theta}{\beta_{SD_f}}\right)^{\alpha_{SD_f}f}. \tag{C.2}$$

Using the inequality $xy/(x+y+1) < \min(x,y)$ [43] and the asymptotic CDF in (20), I_2^∞ can be further expressed as

$$I_2^\infty = 1 - \Pr\left(\frac{\rho_{SR}\gamma_1\left(L_f\rho_{RD_f}\gamma_2/T_f\right)}{\rho_{SR}\gamma_1 + \left(L_f\rho_{RD_f}\gamma_2/T_f\right) + 1} > \frac{L_f\gamma_{thf}}{a_1E_f - \left(a_2E_f + J_f\right)\gamma_{thf}}\right)$$
$$\approx 1 - \Pr\left(\rho_{SR} > \varphi', \rho_{RD_f} > \varphi''\right)$$
$$\approx F_{\rho_{SR}}\left(\varphi'\right) + F_{\rho_{RD_f}}\left(\varphi''\right)$$
$$\approx \frac{\varphi'^{\alpha_{SR}}}{\alpha_{SR}!\beta_{SR}^{\alpha_{SR}}} + \frac{\varphi''^{\alpha_{RD_f}}}{\alpha_{RD_f}!\beta_{RD_f}^{\alpha_{RD_f}}}. \tag{C.3}$$

Substituting (C.2) and (C.3) into (C.1), the asymptotic outage probability of D_f can be obtained.

D. Proof of Corollary 2

Based on (B.1), the asymptotic outage probability of D_n can be expressed as

$$P_{\text{out}}^{D_n,\infty} = I_3^\infty I_4^\infty. \tag{D.1}$$

Similar to (C.2) and (C.3), I_3^∞ and I_4^∞ can be further expressed as

$$I_3^{\infty} = \Pr\left(\rho_{RD_n} < \xi\right) \approx b_n^{\infty}\left(\frac{1}{\alpha_{RD_n}!}\right)^n\left(\frac{\xi}{\beta_{RD_n}}\right)^{n\alpha_{RD_n}}, \quad \text{(D.2)}$$

$$\begin{aligned} I_4^{\infty} &= 1 - \Pr\left(\frac{\rho_{SR}\gamma_1\left(L_n\rho_{RD_n}\gamma_2/T_n\right)}{\rho_{SR}\gamma_1 + \left(L_f\rho_{RD_n}\gamma_2/T_n\right) + 1}\right. \\ &> \frac{L_n\gamma_{thf}}{a_1E_n - (a_2E_n + J_n)\gamma_{thf}}, \frac{\rho_{SR}\gamma_1\left(L_n\rho_{RD_n}\gamma_2/T_n\right)}{\rho_{SR}\gamma_1 + \left(L_f\rho_{RD_n}\gamma_2/T_n\right) + 1} \\ &\left.> \frac{L_n\gamma_{thn}}{a_2E_n - (a_2J_n + a_1\varepsilon E_n)\gamma_{thn}}\right) \\ &\approx 1 - \Pr\left(\rho_{SR} > \tau', \rho_{RD_n} > \tau''\right) \\ &\approx F_{\rho_{SR}}\left(\tau'\right) + F_{\rho_{RD_n}}\left(\tau''\right) \approx \frac{\tau'^{\alpha_{SR}}}{\alpha_{SR}!\beta_{SR}^{\alpha_{SR}}} + \frac{\tau''^{\alpha_{RD_n}}}{\alpha_{RD_n}!\beta_{RD_n}^{\alpha_{RD_n}}}. \end{aligned} \quad \text{(D.3)}$$

Substituting (D.2) and (D.3) into (D.1), the asymptotic outage probability of D_n can be obtained.

Data Availability

All data generated or analyzed during this study are owned by all the authors and will be used to our further research. The data used to support the findings of this study are available from the corresponding author upon request.

Conflicts of Interest

The authors declare that they have no conflicts of interest.

Acknowledgments

This work is supported by the National Natural Science Foundation of China (No. 41904078) and the Science and Technology Research Project of Henan Province of China (No. 202102310560).

References

[1] D. Zhang, Z. Zhou, S. Mumtaz, J. Rodriguez, and T. Sato, "One integrated energy efficiency proposal for 5G IoT communications," *IEEE Internet of Things Journal*, vol. 3, no. 6, pp. 1346–1354, 2016.

[2] K. N. R. S. V. Prasad, E. Hossain, and V. K. Bhargava, "Energy efficiency in massive MIMO-based 5G networks: opportunities and challenges," *IEEE Wireless Communications*, vol. 24, no. 3, pp. 86–94, 2017.

[3] X. Li, J. Li, L. Li, L. Du, J. Jin, and D. Zhang, "Performance analysis of cooperative small cell systems under correlated rician/gamma fading channels," *IET Signal Process*, vol. 12, no. 1, pp. 64–73, 2018.

[4] S. M. R. Islam, N. Avazov, O. A. Dobre, and K. Kwak, "Power-domain non-orthogonal multiple access (NOMA) in 5G systems: potentials and challenges," *IEEE Communication Surveys Tutorials*, vol. 19, no. 2, pp. 721–742, 2017.

[5] D. Wang, D. Chen, B. Song, N. Guizani, X. Yu, and X. Du, "From IoT to 5G I-IoT: the next generation IoT-based intelligent algorithms and 5G technologies," *IEEE Communications Magazine*, vol. 56, no. 10, pp. 114–120, 2018.

[6] 3GPP TR 38.812, "Study on Non-Orthogonal Multiple Access (NOMA) for NR, TSG RAN Meeting 67," 2018, https://www.3gpp.org/DynaReport/TDocExMtg–R1-95–18807.htm.

[7] R. Abozariba, M. K. Naeem, M. Patwary, M. Eyedebrahimi, P. Bull, and A. Aneiba, "NOMA-based resource allocation and mobility enhancement framework for IoT in next generation cellular networks," *IEEE Access*, vol. 7, pp. 29158–29172, 2019.

[8] W. U. Khan, F. Jameel, T. Ristaniemi, B. M. Elhalawany, and J. Liu, "Efficient power allocation for multi-cell uplink NOMA network," in *2019 IEEE 89th Vehicular Technology Conference (VTC2019-Spring)*, pp. 1–5, Kuala Lumpur, Malaysia, Malaysia, April 2019.

[9] L. Dai, B. Wang, Z. Ding, Z. Wang, S. Chen, and L. Hanzo, "A survey of non-orthogonal multiple access for 5G," *IEEE Communications Surveys & Tutorials*, vol. 20, no. 3, pp. 2294–2323, 2018.

[10] W. U. Khan, "Maximizing physical layer security in relay-assisted multicarrier nonorthogonal multiple access transmission," *Internet Technology Letters*, vol. 2, no. 2, 2019.

[11] X. Liu, Y. Wang, S. Liu, and J. Meng, "Spectrum resource optimization for NOMA-based cognitive radio in 5G communications," *IEEE Access*, vol. 6, pp. 24904–24911, 2018.

[12] D. Zhang, Y. Liu, Z. Ding, Z. Zhou, A. Nallanathan, and T. Sato, "Performance analysis of non-regenerative massive-MIMO-NOMA relay systems for 5G," *IEEE Transactions on Communications*, vol. 65, no. 11, pp. 4777–4790, 2017.

[13] Z. Ding, M. Peng, and H. V. Poor, "Cooperative non-orthogonal multiple access in 5G systems," *IEEE Communications Letters*, vol. 19, no. 8, pp. 1462–1465, 2015.

[14] L. Lv, J. Chen, and Q. Ni, "Cooperative non-orthogonal multiple access in cognitive radio," *IEEE Communications Letters*, vol. 20, no. 10, pp. 2059–2062, 2016.

[15] O. Abbasi, A. Ebrahimi, and N. Mokari, "NOMA inspired cooperative relaying system using an AF relay," *IEEE Wireless Communications Letters*, vol. 8, no. 1, pp. 261–264, 2019.

[16] L. Zhang, J. Liu, M. Xiao, G. Wu, Y. Liang, and S. Li, "Performance analysis and optimization in downlink NOMA systems with cooperative full-duplex relaying," *IEEE Journal on Selected Areas in Communications*, vol. 35, no. 10, pp. 2398–2412, 2017.

[17] M. Alkhawatrah, Y. Gong, G. Chen, S. Lambotharan, and J. A. Chambers, "Buffer-aided relay selection for cooperative NOMA in the internet of things," *IEEE Internet of Things Journal*, vol. 6, no. 3, pp. 5722–5731, 2019.

[18] F. Jameel, W. U. Khan, Z. Chang, T. Ristaniemi, and J. Liu, "Secrecy analysis and learning-based optimization of cooperative NOMA SWIPT systems," in *2019 IEEE International Conference on Communications Workshops (ICC Workshops)*, pp. 1–6, Shanghai, China, China, May 2019.

[19] L. P. Qian, A. Feng, Y. Huang, Y. Wu, B. Ji, and Z. Shi, "Optimal SIC ordering and computation resource allocation in MEC-Aware NOMA NB-IoT networks," *IEEE Internet of Things Journal*, vol. 6, no. 2, pp. 2806–2816, 2019.

[20] X. Yan, J. Ge, Y. Zhang, and L. Gou, "NOMA-based multiple-antenna and multiple-relay networks over Nakagami-*m* fading channels with imperfect CSI and SIC error," *IET Communications*, vol. 12, no. 17, pp. 2087–2098, 2018.

[21] X. Li, M. Liu, C. Deng et al., "Joint effects of residual hardware impairments and channel estimation errors on SWIPT assisted cooperative NOMA networks," *IEEE Access*, vol. 7, pp. 135499–135513, 2019.

[22] X. Yue, Z. Qin, Y. Liu, S. Kang, and Y. Chen, "A unified framework for non-orthogonal multiple access," *IEEE Transactions on Communications*, vol. 66, no. 11, pp. 5346–5359, 2018.

[23] G. Im and J. H. Lee, "Outage probability for cooperative NOMA systems with imperfect SIC in cognitive radio networks," *IEEE Communications Letters*, vol. 23, no. 4, pp. 692–695, 2019.

[24] T. Schenk, *RF Imperfections in High-Rate Wireless Systems: Impact and Digital Compensation*, Springer, Netherlands, 2018.

[25] X. Li, J. Li, Y. Liu, Z. Ding, and A. Nallanathan, "Outage performance of cooperative NOMA networks with hardware impairments," in *2018 IEEE Global Communications Conference (GLOBECOM)*, pp. 1–6, Abu Dhabi, United Arab Emirates, December 2018.

[26] A. Gomaa and L. M. A. Jalloul, "Data-aided I/Q imbalance estimation and compensation in OFDM systems," *IEEE Communications Letters*, vol. 18, no. 3, pp. 459–462, 2014.

[27] M. Mokhtar, A. A. Boulogeorgos, G. K. Karagiannidis, and N. Al-Dhahir, "OFDM opportunistic relaying under joint transmit/receive I/Q imbalance," *IEEE Transactions on Communications*, vol. 62, no. 5, pp. 1458–1468, 2014.

[28] A. Gouissem, R. Hamila, and M. O. Hasna, "Outage performance of cooperative systems under IQ imbalance," *IEEE Transactions on Communications*, vol. 62, no. 5, pp. 1480–1489, 2014.

[29] B. Selim, S. Muhaidat, P. C. Sofotasios, A. Al-Dweik, B. S. Sharif, and T. Stouraitis, "Radio-frequency front-end impairments: performance degradation in nonorthogonal multiple access communication systems," *IEEE Vehicular Technology Magazine*, vol. 14, no. 1, pp. 89–97, 2019.

[30] J. Li, M. Matthaiou, and T. Svensson, "I/Q imbalance in two-way AF relaying," *IEEE Transactions on Communications*, vol. 62, no. 7, pp. 2271–2285, 2014.

[31] B. Selim, S. Muhaidat, P. C. Sofotasios et al., "Performance analysis of nonorthogonal multiple access under I/Q imbalance," *IEEE Access*, vol. 6, pp. 18453–18468, 2018.

[32] J. Li, M. Matthaiou, and T. Svensson, "I/Q imbalance in AF dual-hop relaying: performance analysis in Nakagami-*m* fading," *IEEE Transactions on Communications*, vol. 62, no. 3, pp. 836–847, 2014.

[33] X. Li, M. Liu, C. Deng, P. T. Mathiopoulos, Z. Ding, and Y. Liu, "Fullduplex cooperative NOMA relaying systems with I/Q imbalance and imperfect SIC," *IEEE Wireless Communications Letters*, vol. 9, no. 1, pp. 17–20, 2020.

[34] X. Li, Q. Wang, H. Peng et al., "A unified framework for HS-UAV NOMA networks: performance analysis and location optimization," *IEEE Access*, vol. 8, pp. 13329–13340, 2020.

[35] M. Chraiti, A. Ghrayeb, and C. Assi, "A NOMA scheme for a two-user MISO downlink channel with unknown CSIT," *IEEE Transactions on Wireless Communications*, vol. 17, no. 10, pp. 6775–6789, 2018.

[36] X. Li, J. Li, Y. Liu, Z. Ding, and A. Nallanathan, "Residual transceiver hardware impairments on cooperative NOMA networks," *IEEE Transactions on Wireless Communications*, vol. 19, no. 1, pp. 680–695, 2020.

[37] H. Haci, H. Zhu, and J. Wang, "Performance of non-orthogonal multiple access with a novel asynchronous interference cancellation technique," *IEEE Transactions on Communications*, vol. 65, no. 3, pp. 1319–1335, 2017.

[38] X. Yue, Y. Liu, S. Kang, and A. Nallanathan, "Performance analysis of NOMA with fixed gain relaying over Nakagami-*m* fading channels," *IEEE Access*, vol. 5, pp. 5445–5454, 2017.

[39] J. Men, J. Ge, and C. Zhang, "Performance analysis for downlink relaying aided non-orthogonal multiple access networks with imperfect CSI over Nakagami-*m* fading," *IEEE Access*, vol. 5, pp. 998–1004, 2017.

[40] X. Li, M. Liu, D. Deng, J. Li, C. Deng, and Q. Yu, "Power beacon assisted wireless power cooperative relaying using Noma with hardware impairments and imperfect CSI," *AEU - International Journal of Electronics and Communications*, vol. 108, pp. 275–286, 2019.

[41] X. Li, J. Li, and L. Li, "Smart home monitoring system via footstep-induced vibrations," *IEEE Systems Journal*, vol. 2019, pp. 1–7, 2019.

[42] Z. Zhou, C. Gao, C. Xu, T. Chen, D. Zhang, and S. Mumtaz, "Energy efficient stable matching for resource allocation in energy harvesting based device-to-device communications," *IEEE Access*, vol. 5, pp. 15184–15196, 2017.

[43] P. A. Anghel and M. Kaveh, "Exact symbol error probability of a cooperative network in a rayleigh-fading environment," *IEEE Transactions on Wireless Communications*, vol. 3, no. 5, pp. 1416–1421, 2004.